ELECTRONIC SUPPLEMENTARY MATERIAL APPENDIX A:

Supplementary Notes and Images

NOTE 1: SEISMOGENIC SOURCE MODELS
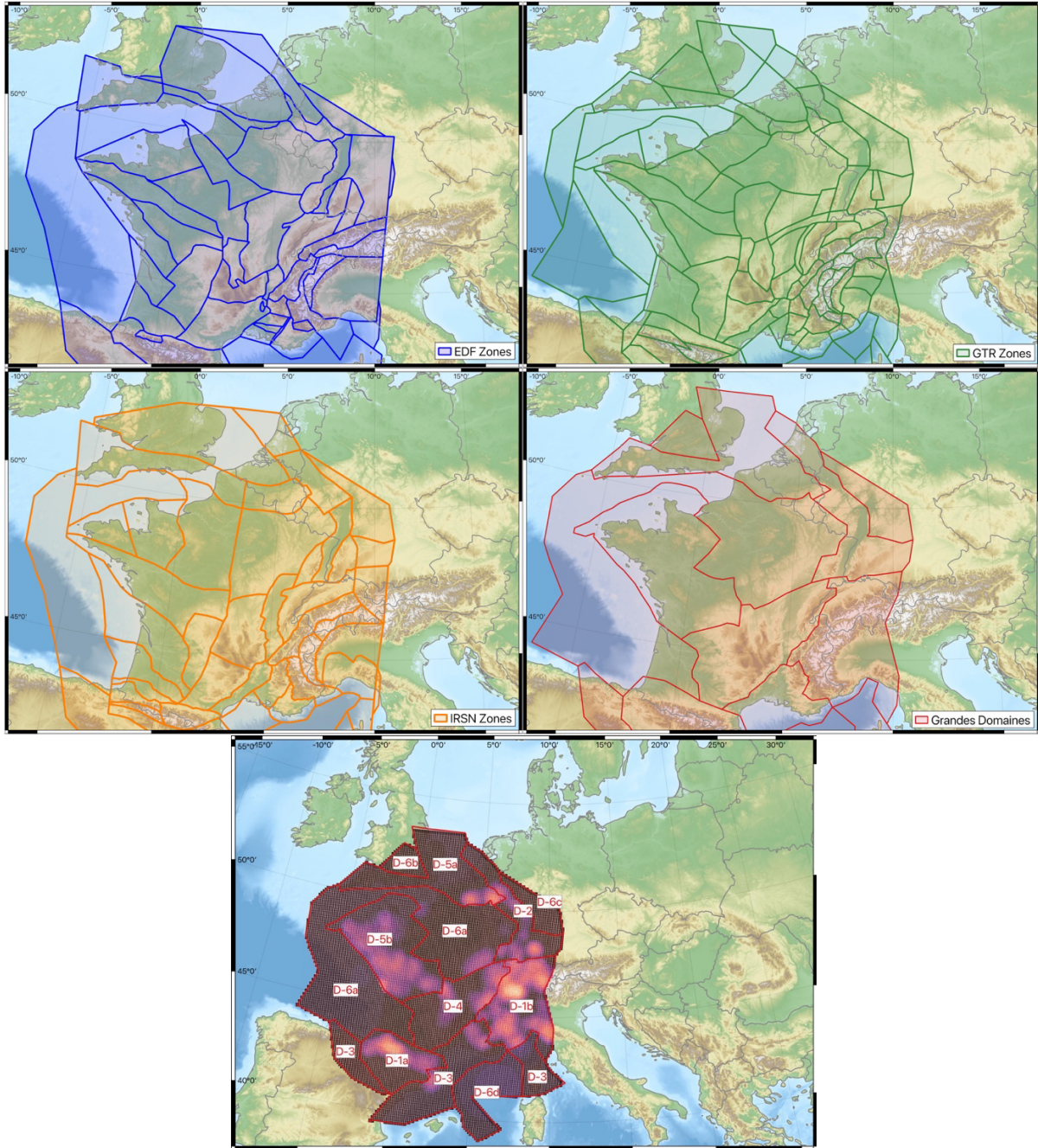
Figure S1: Seismogenic area source zonations adopted for France by Drouet et al. (2020): EDF (top left), GTR (top right), IRSN (middle left) and a larger scale "Grands Domaines" model (middle right) used to determine activity rate parameters β and M_{MAX} for the zoneless (smoothed seismicity) source model (bottom)
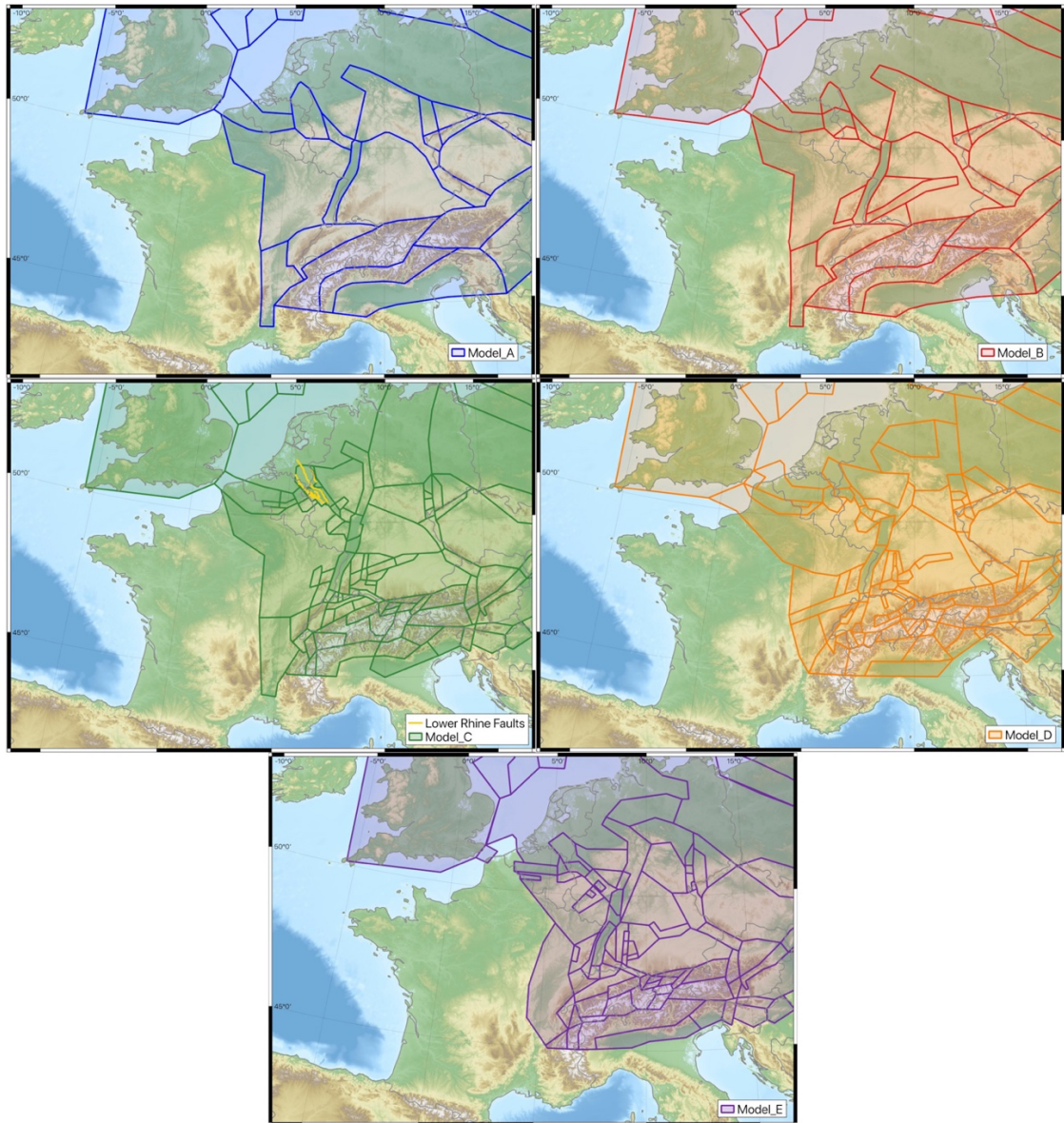
Figure S2. Seismic source model branches adopted for DE2016 (Grünthal et al., 2018): Model A (top left), Model B (top right), Model C with Active Faults shown (middle left), Model D (middle right) and Model E (bottom)
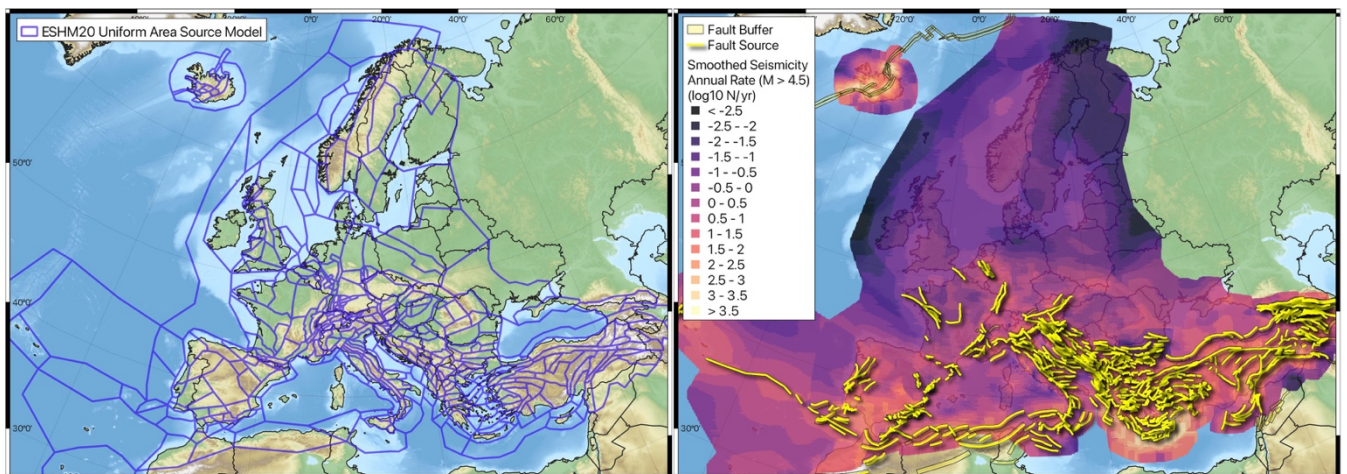
Figure S3. Seismic sources adopted within ESHM20: uniform area source model (left), fault source and smoothed seismicity model (right)

NOTE 2: Sampling in Drouet et al. (2020) Magnitude Frequency Relations (MFRs)

Although Drouet et al. (2020) indicate that epistemic uncertainty in MFRs is evaluated by the Monte Carlo sampling process, the translation of the model into OpenQuake (see section 3) revealed details of the sampling process that were not described in the original literature. The authors of the model provided the sets of original samples, which revealed that a stratified sampling process had been adopted, which is illustrated for a single source (GTR – FRS) in Figure S4. The sampled a and b values used for the calculation logic tree (red dots) are compared against a set of 10,000 samples from a multivariate normal distribution (blue crosses). In their sampling process Drouet et al. (2020) discretised the marginal b-value distribution into a fixed set of bins, the number of samples in the bin being proportional to the density of the bin. Then for each bin the a values are sampled from the marginal distribution conditional on each b-value (Gabriele Ameri, *personal comm.*). For each of the source zones in each source model, we run a multivariate analysis of variance (MANOVA) on the distribution of sampled values for each of the zones and find that in the vast majority cases we cannot reject the null hypothesis that the sample a and b values are drawn from the underlying multivariate Gaussian distribution. The same exploration of the sampled values showed that a similar stratified sampling approach was used for $f(M_{MAX})$ with fixed M_{MAX} bins sampled according to the posterior probability density from the EPRI approach.
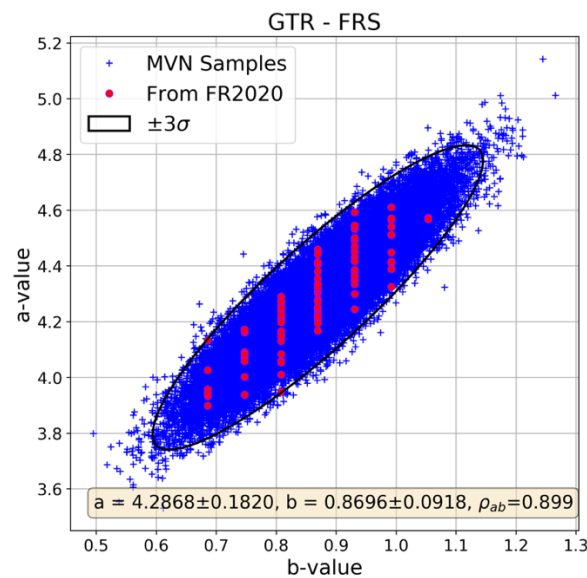
Figure S4. Example of sampled a and b values for a single zone (GTR – FRS). The $\pm 3\sigma$ error ellipse is shown in black; the blue crosses indicate the distribution of 10,000 samples from a multivariate normal distribution and the red dots the 100 samples for the zone used by Drouet et al. (2020)

NOTE 3: OpenQuake Source Model Characterisation – Source Types and Model Needs

In the seismic source models for the three models described in section 2, we encounter three types of sources: i) uniform area zones, ii) smoothed seismicity (manifesting as gridded seismicity) and iii) active faults with exponential recurrence models. The first two of these would be described as *distributed seismicity* sources as the earthquakes are not associated to a specific seismogenic fault but instead are distributed uniformly within a region (for the area zones) or anchored to a specific location in a fine grid cell (for gridded seismicity). For the active fault sources in the Upper Rhine Graben (ESHM20) and Lower Rhine Graben (ESHM20 and DE2016) the type of recurrence model is relevant even when the fault surfaces themselves are broadly consistent between different

models. With exponential recurrence the rupture size of a large proportion of the earthquakes considered will be smaller than the full area of the fault. Therefore, these smaller ruptures must be distributed across the fault surface ("floating the ruptures"), which is assumed to occur uniformly (i.e., each rupture location is equally probable).

The seismogenic source model may describe the location and recurrence of the earthquakes, but it is the ground motion model (GMM) that sets the requirements of how the rupture is parameterized in order to determine the distribution of ground motions at a location. Here the GMMs typically require distance metrics that relate to the three-dimensional finite rupture surface (e.g., closest distance to rupture, R_{RUP}, or distance to the surface projection of the rupture, R_{JB} or Joyner-Boore distance). Depending on the PSHA software magnitude-dependent rupture size in distributed seismicity sources is accommodated either by the use of *virtual faults* (e.g., Bommer & Akkar, 2012; Monelli et al., 2014; Bommer & Montaldo Falero, 2020) or by empirical (or semi-analytical) adjustments to the point-source distances (e.g., epicentral distance, R_{EPI}, and hypocentral distance, R_{HYPO}) dependent on earthquake magnitude (e.g. Scherbaum et al., 2004; Thompson & Worden, 2018). OpenQuake adopts the *virtual faults* approach, meaning that for distributed seismicity sources information is needed to define the hypocentral depths, the rupture orientations (strike and dip) and styles of faulting (rake), rupture length to width ratio (aspect ratio), magnitude to rupture area scaling relation and seismogenic thickness of the source. The distributions of hypocentral depth and rupture nodal plane (strike, dip and rake) are specified as probability mass functions, while aspect ratio, scaling relation and seismogenic thickness are set for each source. If the vertical extent of the rupture width for an event of given magnitude, area and aspect ratio exceeds the seismogenic thickness, the rupture is rescaled to allow a larger aspect ratio while still conserving total area. Further details can be found in Pagani et al. (2014a, b).

For active faults with rupture areas less than the total area of the fault, OpenQuake requires additional information to control the dimension of the 3D "floating ruptures" for the given magnitude, and their distribution across the fault surface. Though the strike, dip and rake of the ruptures are constrained by the 3D fault surface, the rupture area for each magnitude is defined from a magnitude to area scaling relation, along with an initial aspect ratio. As for the distributed seismicity sources, if the rupture width for a given magnitude and aspect ratio exceeds the total width of the fault surface, the rupture width is fixed to the fault width while the length is increased in order to conserve rupture area at the expense of aspect ratio.

The brief descriptions of how the finite fault rupture for each earthquake must be characterized in OpenQuake, and what is therefore required from the hazard modeler to input, are illustrative of both the irreconcilable discrepancies between PSHA software and of the free parameters/modelling choices. The differences may be irreconcilable because alternative PSHA software may adopt different approaches for finite rupture characterization in both distributed seismicity and active fault sources from that of the virtual faults used by OpenQuake. The free parameters/modelling choices emerge, however, as different software may allow the user control of some, or all, of the information needed to make these corrections. In the following descriptions of the migration process we will highlight where sufficient information on the model configurations was available to allow for direct reproduction of the behaviour of the original software within the OpenQuake framework and where alternative decisions or interpretations had to be made.

NOTE 4: Implementing the FR2020 Model into OpenQuake

As presented in Section 2, FR2020 boasts three uniform area source models (GTR, EDF and IRSN) and one zoneless smoothed seismicity model, for each source model capturing uncertainty in the MFR by drawing 100 samples from the underlying distributions of a, b and M_{MAX}. Documentation of the model is found in the journal paper and electronic supplement of Drouet et al. (2020), along with a detailed technical published by Fugro (GEOTER, 2017). Digital data files were kindly provided to us by the original authors, including the source model geometries, the original sample a, b and M_{MAX} values for the area sources, the original sample M_{MAX} values for the zoneless source, and a comprehensive suite of PSHA hazard curves including all LT branches for 5 selected cities (Brest, Lourdes, Grenoble, Marseille and Nice) as well as the mean and quantile branches for the original 6,836 calculated locations spaced every 0.1˚N by 0.1˚E within the French metropolitan territory. These digital files were critical to the successful migration of the model, yet even then further clarifications several key points were needed from the authors. A complete description of the migration of FR2020 from the original software to OpenQuake can be found in Weatherill et al. (2022), including a complete set of comparisons (both branch by branch and for the mean and quantiles) and detailed discussion and sensitivity analysis of the configurable parameters. Briefly, however, key results that emerged from this process were as follows:

1) Drouet et al. (2020) provided information to constrain the geometry, magnitude frequency distribution, hypocentral depth distribution and seismogenic thickness of the virtual faults for the uniform area sources and gridded seismicity sources, which could be readily adopted in OpenQuake. Magnitude scaling relation and aspect ratio were not provided in the available documentation; however, the authors clarify that the Wells & Coppersmith (1994) relation was used, and that aspect ratio is taken as that implied by the magnitude-length and magnitude-width scaling relations. The same relation was adopted in OpenQuake and a fixed aspect ratio of 1.25 was used, which applies at all magnitudes as the rupture width predicted for M_{MAX} was still within the 29.9 km seismogenic thickness. Rupture orientation and style of faulting distributions were available from the documentation; however, in the original software these were sampled randomly within a range, while in OpenQuake these are distributed evenly within the range by four strike values and one mid-point dip value.

2) Using the sampled a, b and M_{MAX} values it was possible to achieve excellent agreement in the two implementations for the uniform area source zones. We noted, however, that the sampling process (described in section 2) was not documented, and that agreement could not be achieved when drawing new samples from the same distributions using a non-stratified sampling process.

3) The GMM of Ameri (2014) was used for the calculation rather than Ameri et al. (2017). Though the models are similar (Drouet et al., 2020), Ameri (2014) adopts a homoscedastic aleatory uncertainty term and scales differently at very short distances. Ameri (2014) is therefore needed to reproduce the model and the two models cannot be used interchangeably.

4) Contrary to the description of the MFR epistemic uncertainties for the zoneless sources given in the supporting literature for the model (and shown in Figure 1), a and b values *were* sampled randomly for the gridded sources and not just M_{MAX}. In their description of the zoneless model, b and σ_b were defined for each cell from the domains superzones (as was M_{MAX}), while a and σ_a vary cell-by-cell depending on the rate. Further discussion with the modellers revealed that at each cell i for each branch j of $j = 1, 2, \dots 100$ branches $a_{i,j} = a_i + \varepsilon_{i,j}\sigma_{a_i}$ and $b_{i,j} = b_i + \varepsilon_{i,j}\sigma_{b_i}$, where $\varepsilon_{i,j} = \mathcal{N}(\mu = 0, \sigma = 1)$ truncated

between ± 3 standard deviations and the same value $\varepsilon_{i,j}$ is applied to both the $a_{i,j}$ and $b_{i,j}$ samples. With this information it was possible to replicate the variance in the branches of the zoneless model, but the mean values of the zoneless branches is still notably higher in the OpenQuake implementation than in the original curves. At the time of writing, no clear cause for this discrepancy has been found.

NOTE 5: Implementing the DE2016 Model into OpenQuake

The migration of the DE2016 model into OpenQuake begins from a good position as both the calculation input files and proprietary source code are available to the authors. This allows us to retrieve the exact values input into the calculation and to get an understanding of the mechanics of the calculations in the respective software in order to identify what are irreconcilable differences and what can be configured by the user. From a source typology perspective there are many similarities between the FR2020 and DE2016 as both are using uniform area zones and zoneless smoothed seismicity. As the available input files are available to us the source geometries of the uniform area sources are taken directly, along with the hypocentral depth distribution, style-of-faulting probability distribution and the magnitude frequency distributions for all 20 MFR branches. Concurrently, all required GMMs were implemented into the OpenQuake-engine (or existed there prior to this effort) and these implementations were extended to include configurable stress drop adjustment factors. A Germany-specific magnitude-area scaling relation was also added:

$$\log_{10} A = -2.44 + 0.59 \cdot M_W \pm \sigma_{\log_{10} A} \qquad \text{where } \sigma_{\log_{10} A} = 0.16 \qquad (1)$$

Though many aspects of the model could be directly translated into OpenQuake, there are several key differences. For the uniform area sources and the smoothed seismicity, point source to site distances (R_{JB} and R_{RUP}) are used rather than finite ruptures. Three of the GMMs selected (Akkar et al., 2014; Bindi et al. 2014 and Bindi et al., 2017) have versions of the models with coefficients calibrated with respect to a point-source distance, but for Derras et al. (2014) and Cauzzi et al. (2015) finite-rupture distances are needed, and these are converted from point-source distances using empirical conversion models from Scherbaum et al. (2004). No adjustments to the GMM aleatory variability are applied. Adopting point-source distances in the distributed seismicity sources effectively renders the parameters controlling the finite rupture dimension and orientation irrelevant, and only the depth distribution and style-of-faulting (rake) remain relevant. This behaviour, though a fundamental difference in software approaches, was possible to mimic in the OpenQuake-engine.

For the fault sources with exponential recurrence both PSHA software codes (original and OpenQuake) implement rupture floating with uniform distributions both along-strike and down dip. In the original code, magnitude scaling is given according to the formula shown in equation 1, and aspect ratio is fixed 1.0 for ruptures smaller than the fault width but re-scales when the rupture size reaches the maximum down dip width. Where the original PSHA code differs from OpenQuake is that it also integrates the uncertainty in the magnitude scaling relation, while OpenQuake uses only the median value. The relevance of this distinction and its influence on seismic hazard has also been identified and discussed by Allen et al. (2020). A last point that remains unclear, however, is how the point source distances for those GMMs requiring them are retrieved from the rupture surface. We assume that the rupture centroid is used in this case, which is also the default behaviour in OpenQuake.

A final point of note on the DE2016 implementation relates to the smoothed seismicity model. In the original calculations of DE2016 these were in fact implemented in a different PSHA software, a customized script constructed by the authors to combine the approach described by Woo (1996) with the selected GMMs. In this process for each earthquake considered in the catalogue a dynamic mesh of point sources is constructed that is centered on each earthquake epicentre, the corresponding earthquake rate (the inverse of the completeness duration for that magnitude and location) is then distributed across the dynamic mesh according to the smoothing kernel. This process is difficult to replicate in OpenQuake, and results in massive numbers of point sources each with trivially small rates. In the migration process, however, a fixed mesh of point sources is adopted and the rates for each event smoothed across this fixed mesh. The resolution of the fixed mesh is $0.05° \times 0.05°$, and we find the differences in the two approaches to have a negligible impact on the results.

ELECTRONIC SUPPLEMENTARY MATERIAL APPENDIX B:

Seismic Hazard Model Implementation Comparisons – OpenQuake and Original Software

In this supplement we show images comparing the results of the seismic hazard analysis undertaken using the OpenQuake implementation of the Drouet et al. (2020) (FR2020) and Grünthal et al. (2018) (DE2016) models against results obtained from the original PSHA software. For each of the two cases we show the mean seismic hazard maps and the difference maps (in terms of percent (%) increase/decrease) for the 475 year return periods at three different spectral periods (Sa (0.01 s)/PGA, Sa (0.2 s), Sa (1.0 s)). Then for selected cities we show the resulting seismic hazard curves for these three spectral periods and plot the percentage change between the two.

For France, the original seismic hazard results were produced using proprietary software owned by Fugro and made available courtesy of Stéphane Drouet. For Germany, the original seismic hazard results were produced in a proprietary software (a customised version of FRISK) managed and maintained by GFZ (courtesy of Christian Bosse). Maps and curves are compared in terms of probability of exceedance (annual for the curves, 10 % in 50 year for the maps) with median and quantile curves obtained with respect to the distribution of probabilities of exceedance for fixed intensity measure levels (ground motion values). In both cases a reference rock site of V_{S30} 800 m/s is assumed.

FR2020 (Drouet et al., 2020)

Figure S5. Location of target cities in France: Brest, Lourdes, Grenoble, Marseille and Nice
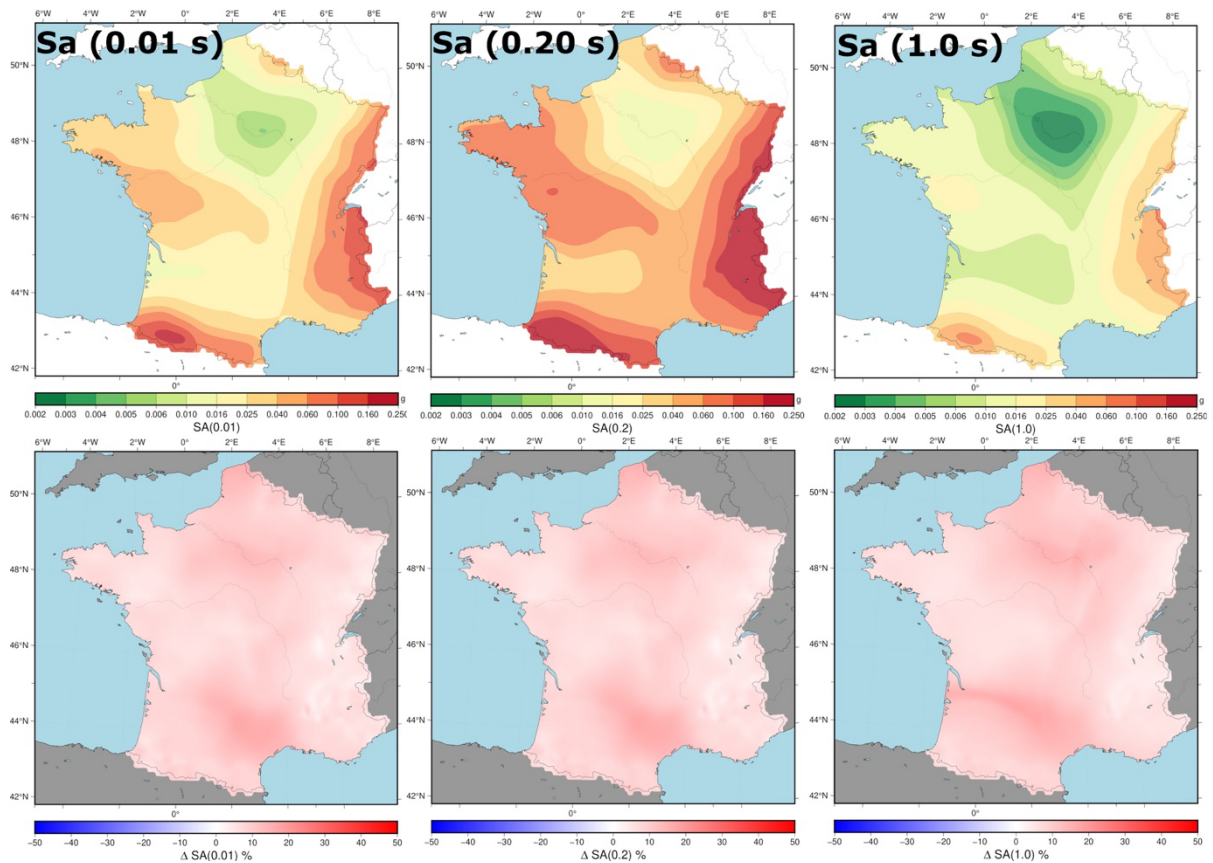
Figure S6. Seismic hazard for FR2020 with a 10 % probability of exceedance in 50 years (top row) for intensity measures Sa (0.01 s) [left], Sa (0.2 s) [middle] and Sa (1.0 s) [right], and relative difference between the OpenQuake implementation and the original software implementation (bottom row).

Figures S7 – S11. (left): Seismic hazard curves for Sa (0.01 s) [upper], Sa (0.2 s) [middle] and Sa (1.0 s) [lower] for the respective city shown in terms of the mean (continuous line) and 16th, 50th and 84th percentiles (dashed lines) for the OpenQuake implementation (red) and original FR2020 software implementation (blue). (right): Percent change Annual Probability of Exceedance (APoE) between the OpenQuake implementation and original software with the target region (± 10 % for 1 x 10-4 ≤ APoE ≤ 1) indicated in shaded blue.
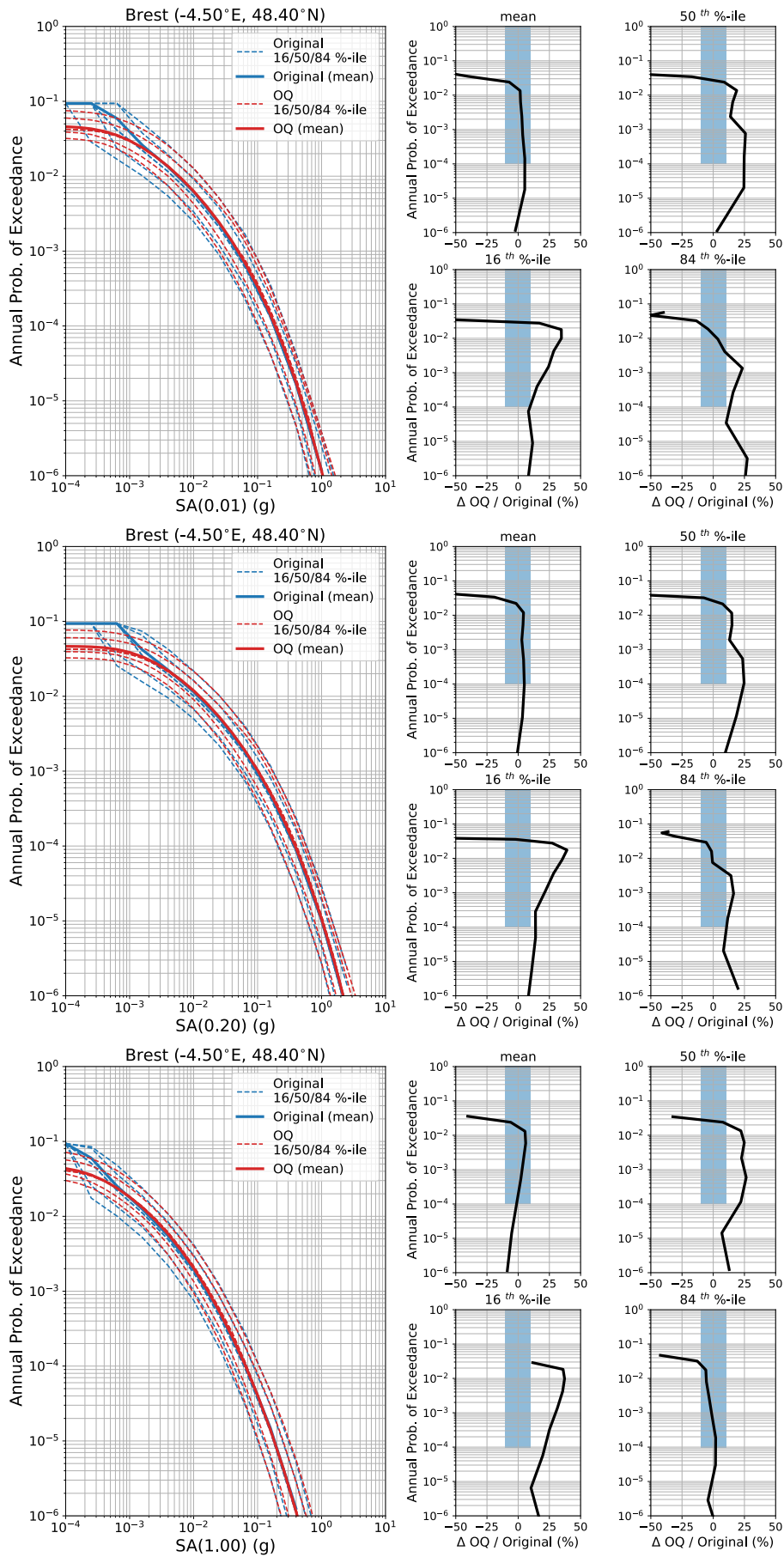
Figure S7. Brest (-4.5˚E, 48.4˚N)
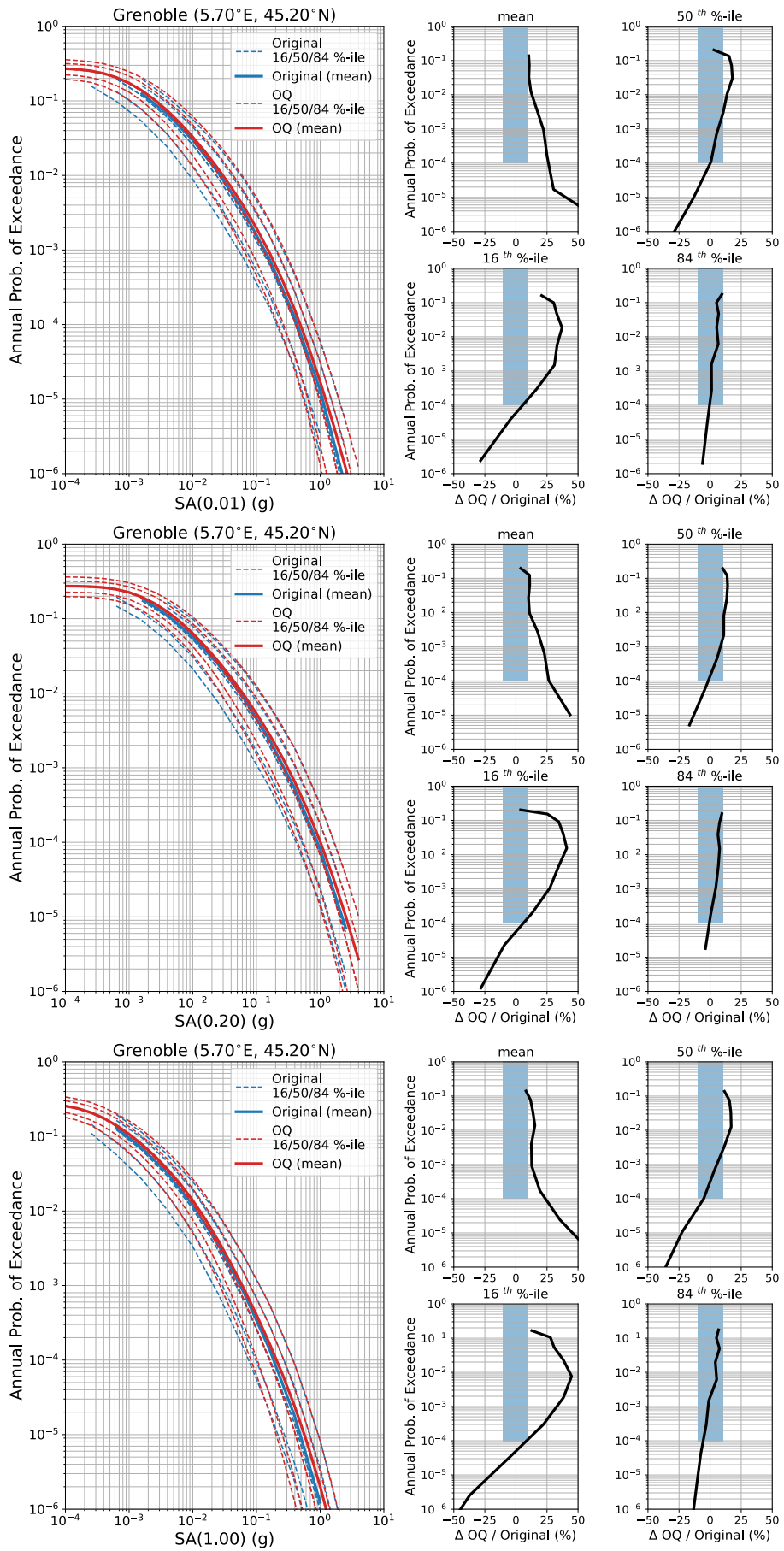
Figure S8. Grenoble (5.70°E, 45.20°N)
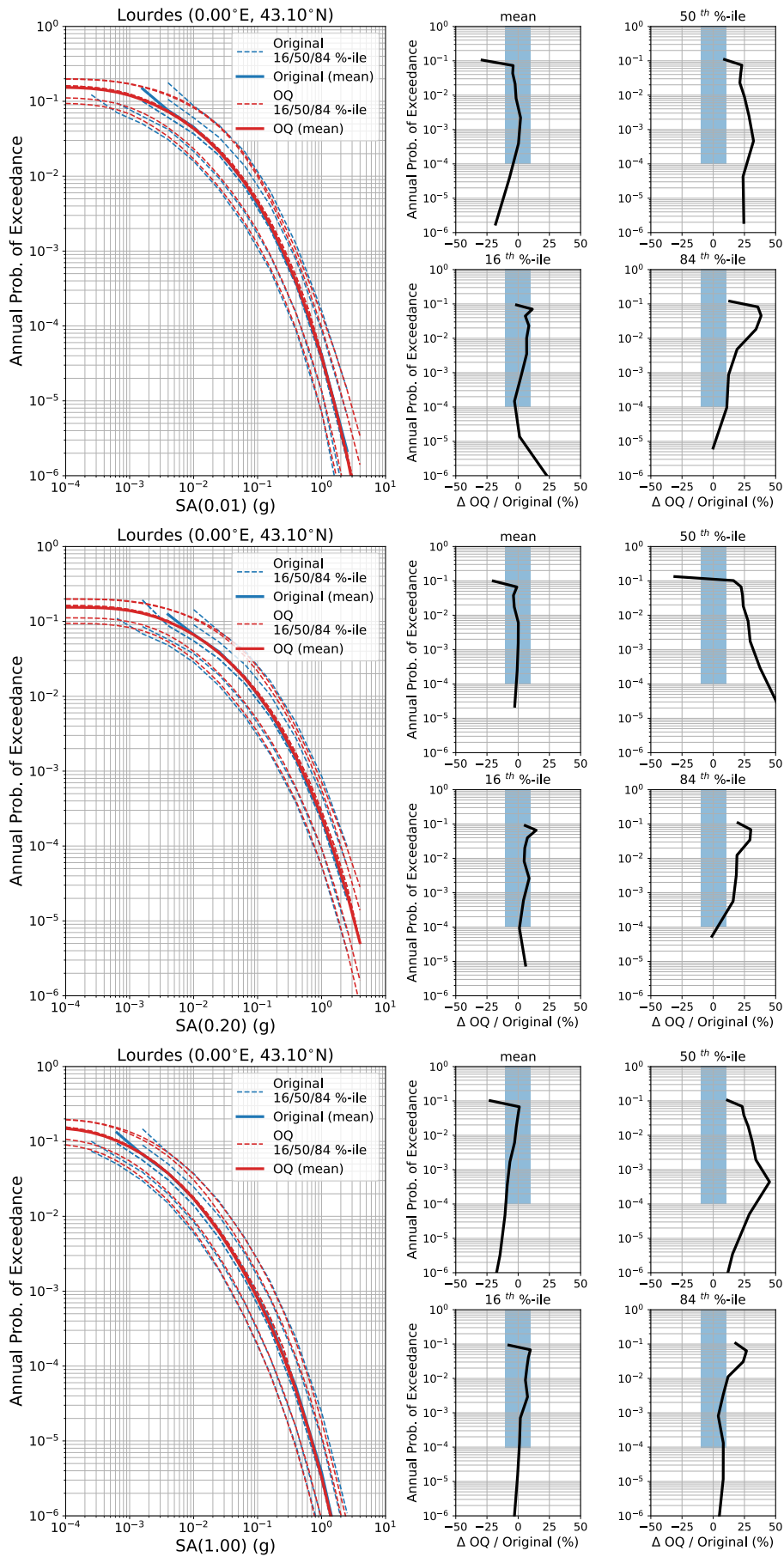
Figure S9. Lourdes (0.00°E, 43.10°N)
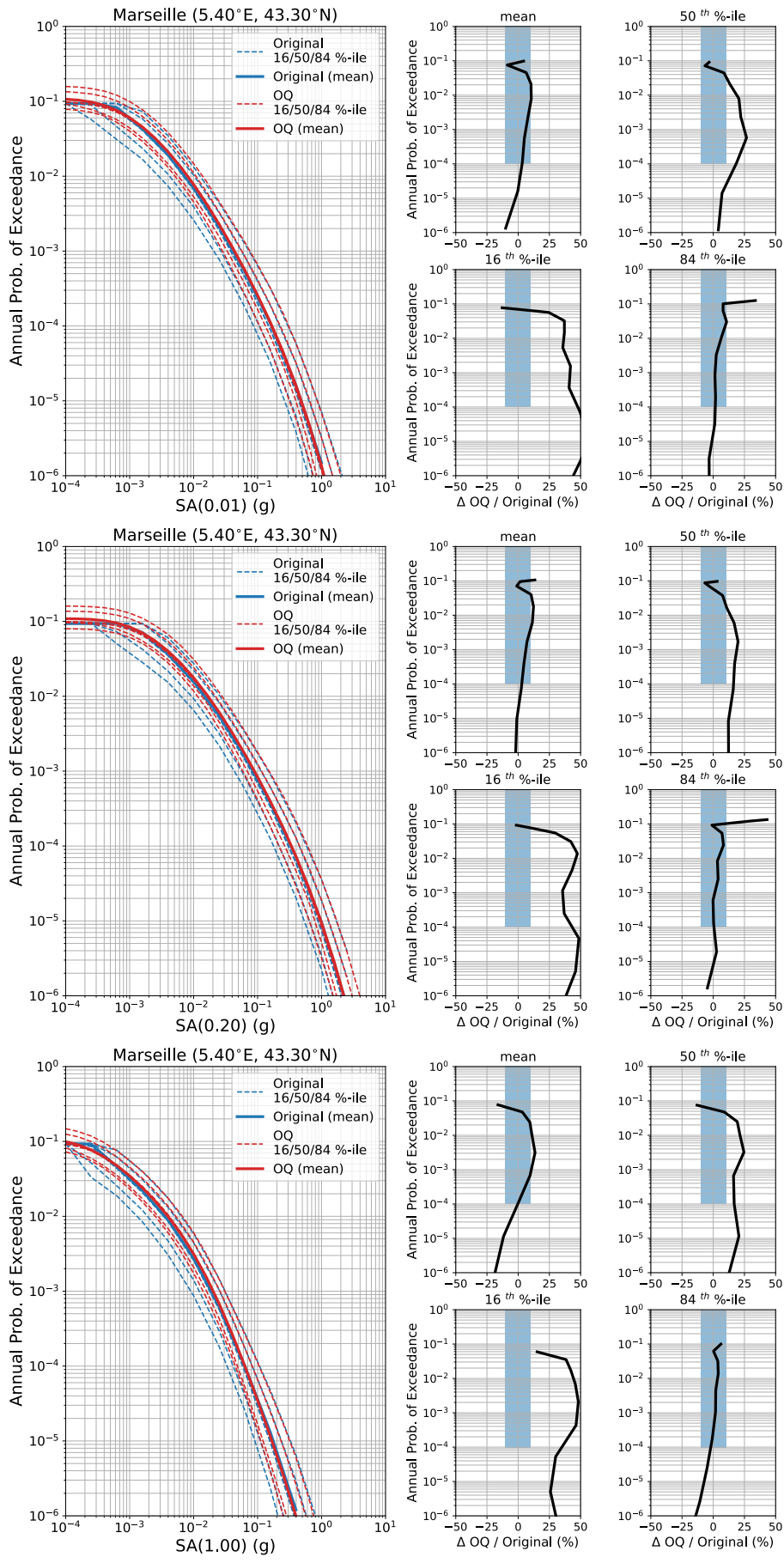
Figure S10. Marseille (5.40˚E, 43.30˚N)
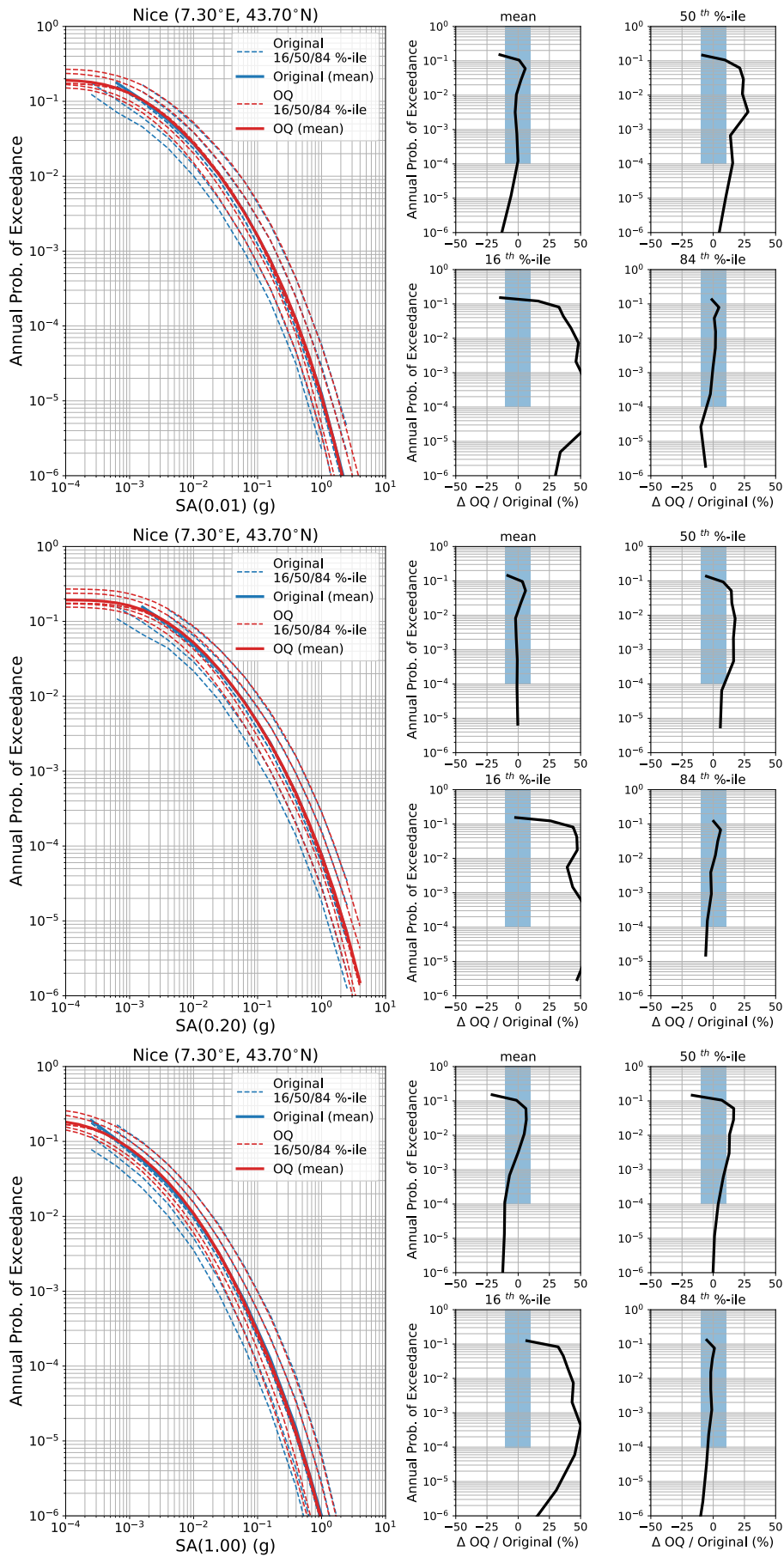
Figure S11. Nice (7.30˚E, 43.70˚N)

DE2016 (Grünthal et al., 2018)

Figure S12. Location of target cities in Germany: Aachen, Cologne, Saarbrücken, Karslruhe, Albstadt and Leipzig

Note: In Figure S13. the largest difference between the two models can be seen in the very low hazard region of northern Germany where the OpenQuake implementation is more than 50 % lower than the original. This difference emerges due to the choice of minimum ground motion intensity measure level set in the input configuration files, which was 0.001 g for the original software and 0.0005 g in the OpenQuake implementation. This results in "clipping" such that the original software has a water level of 0.001 g, while OpenQuake sets this at 0.0005 g. The differences appear large in terms of relative change, but the level of hazard in the affected regions is so low as to render this trivial for any practical application.
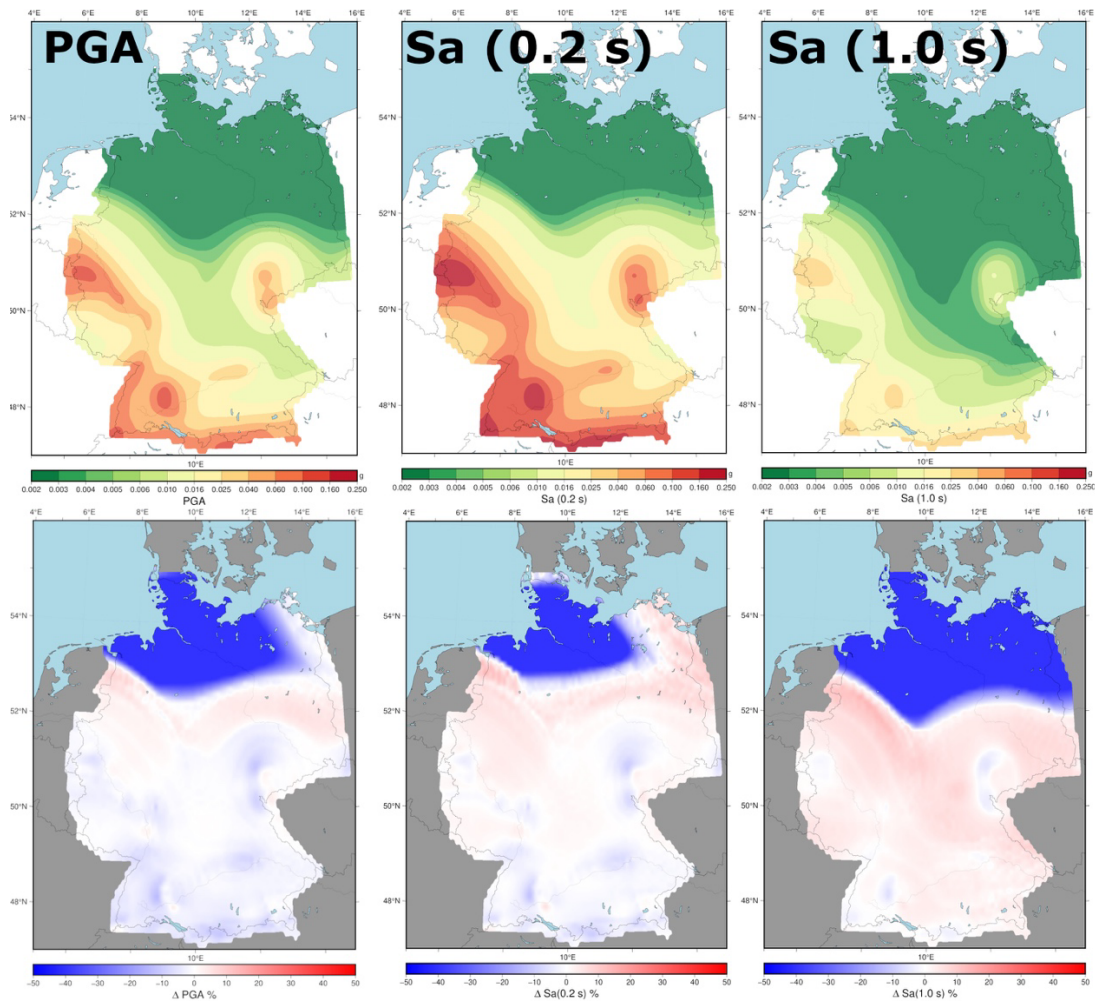
Figure S13. Seismic hazard for DE2016 with a 10 % probability of exceedance in 50 years (top row) for intensity measures PGA [left], Sa (0.2 s) [middle] and Sa (1.0 s) [right], and relative difference between the OpenQuake implementation and the original software implementation (bottom row).

Figures S14 – S19. (left): Seismic hazard curves for Sa (0.01 s) [upper], Sa (0.2 s) [middle] and Sa (1.0 s) [lower] for the respective city shown in terms of the mean (continuous line) and 16th, 50th and 84th percentiles (dashed lines) for the OpenQuake implementation (red) and original DE2016 software implementation (blue). (right): Percent change Annual Probability of Exceedance (APoE) between the OpenQuake implementation and original software with the target region (± 10 % for $1 \times 10^{-4} \leq APoE \leq 1$) indicated in shaded blue.
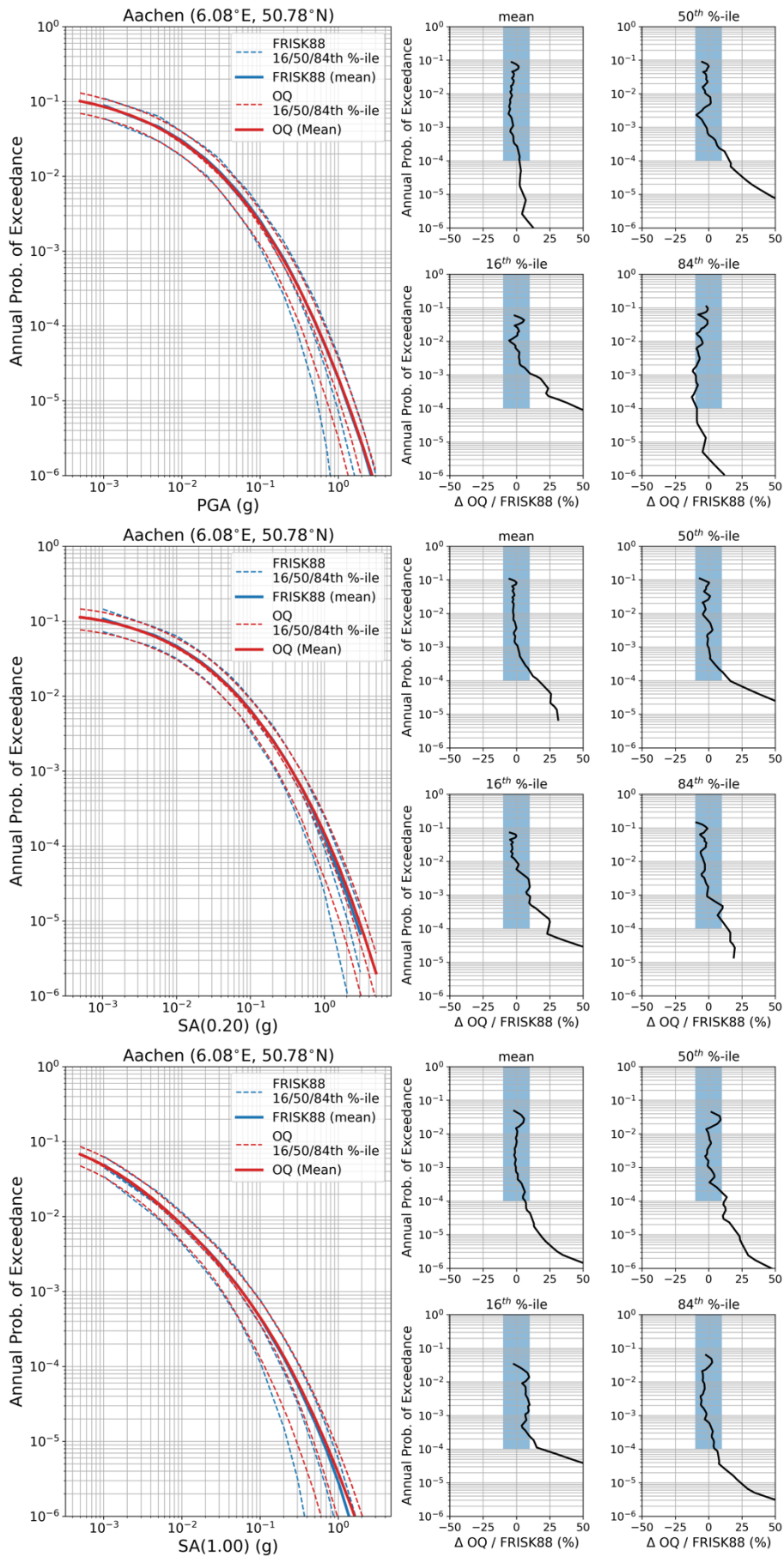
Figure S14. Aachen (6.08°E, 50.78°N)
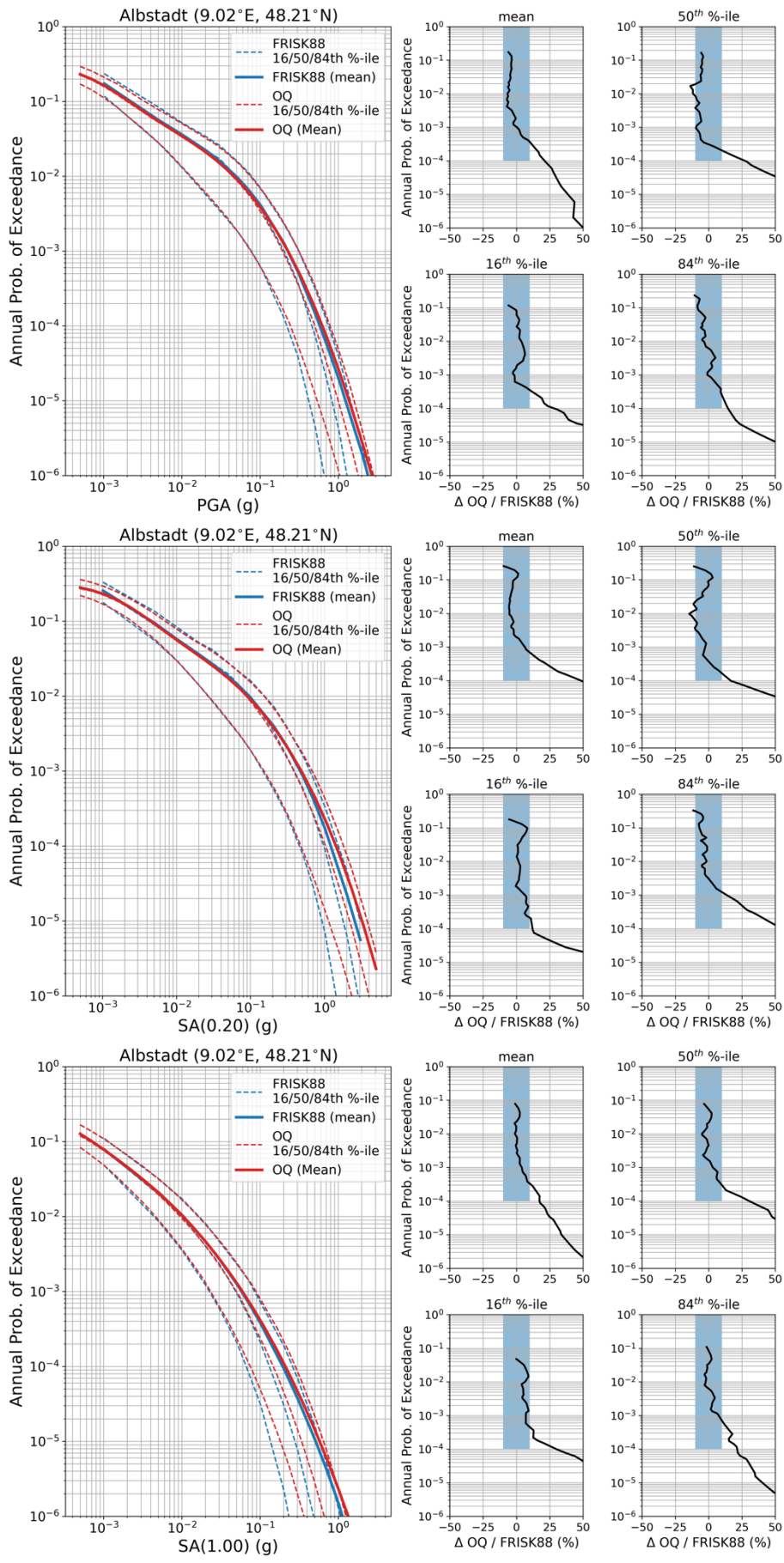
Figure S15. Albstadt (9.02°E, 48.21°N)
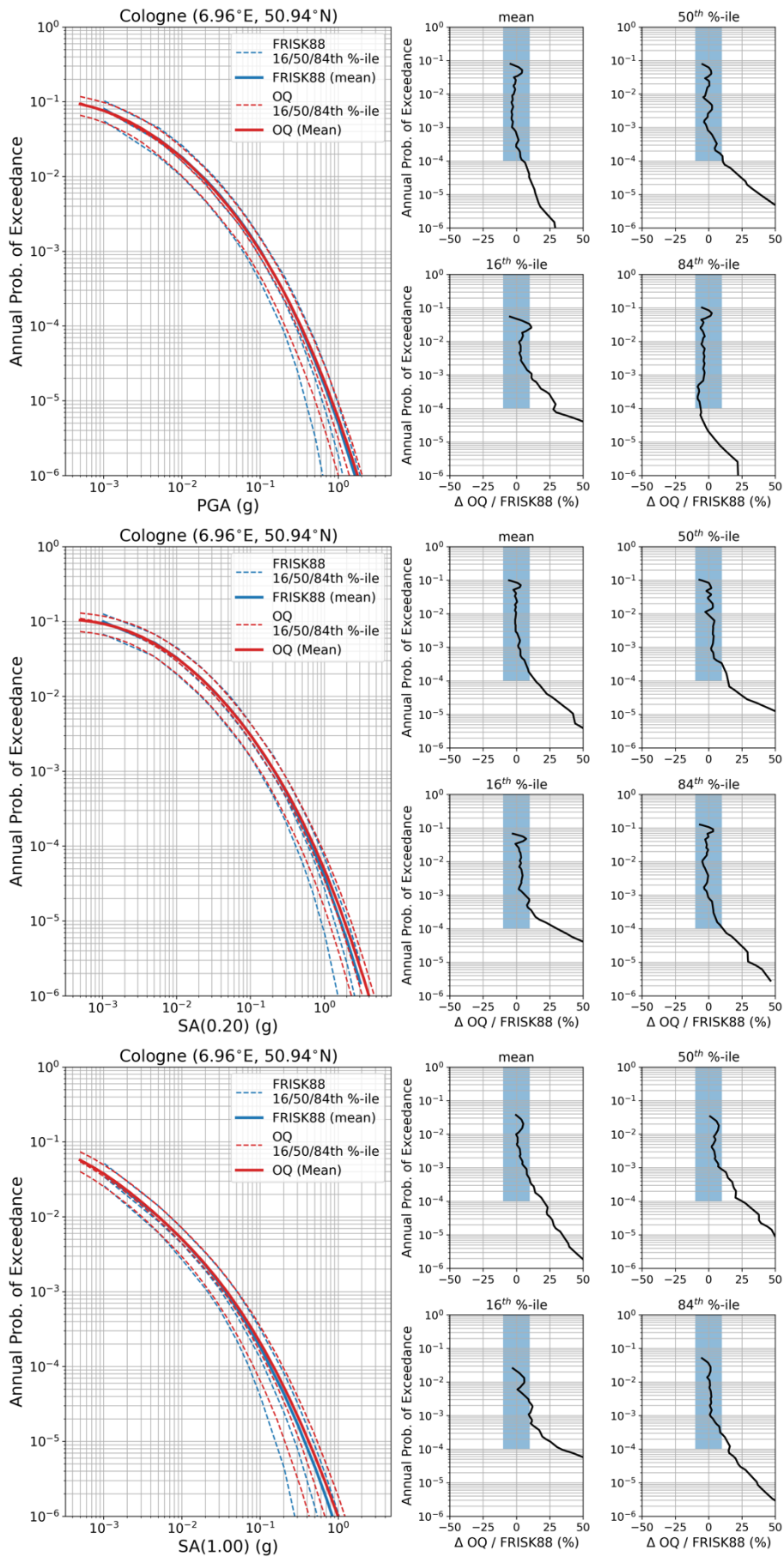
Figure S16. Cologne (6.96°E, 50.94°N)
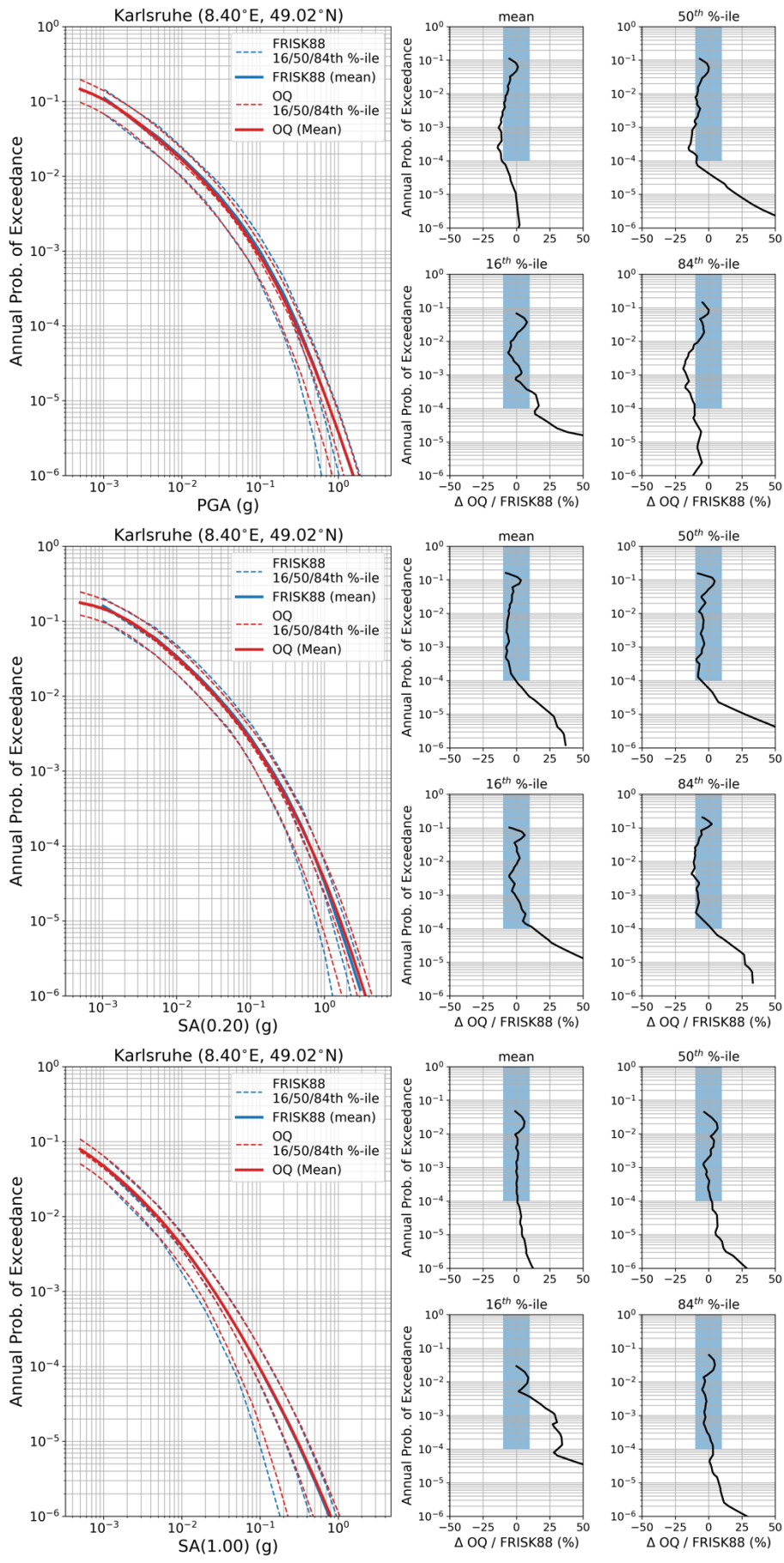
Figure S17. Karlsruhe (8.40°E, 49.02°N)
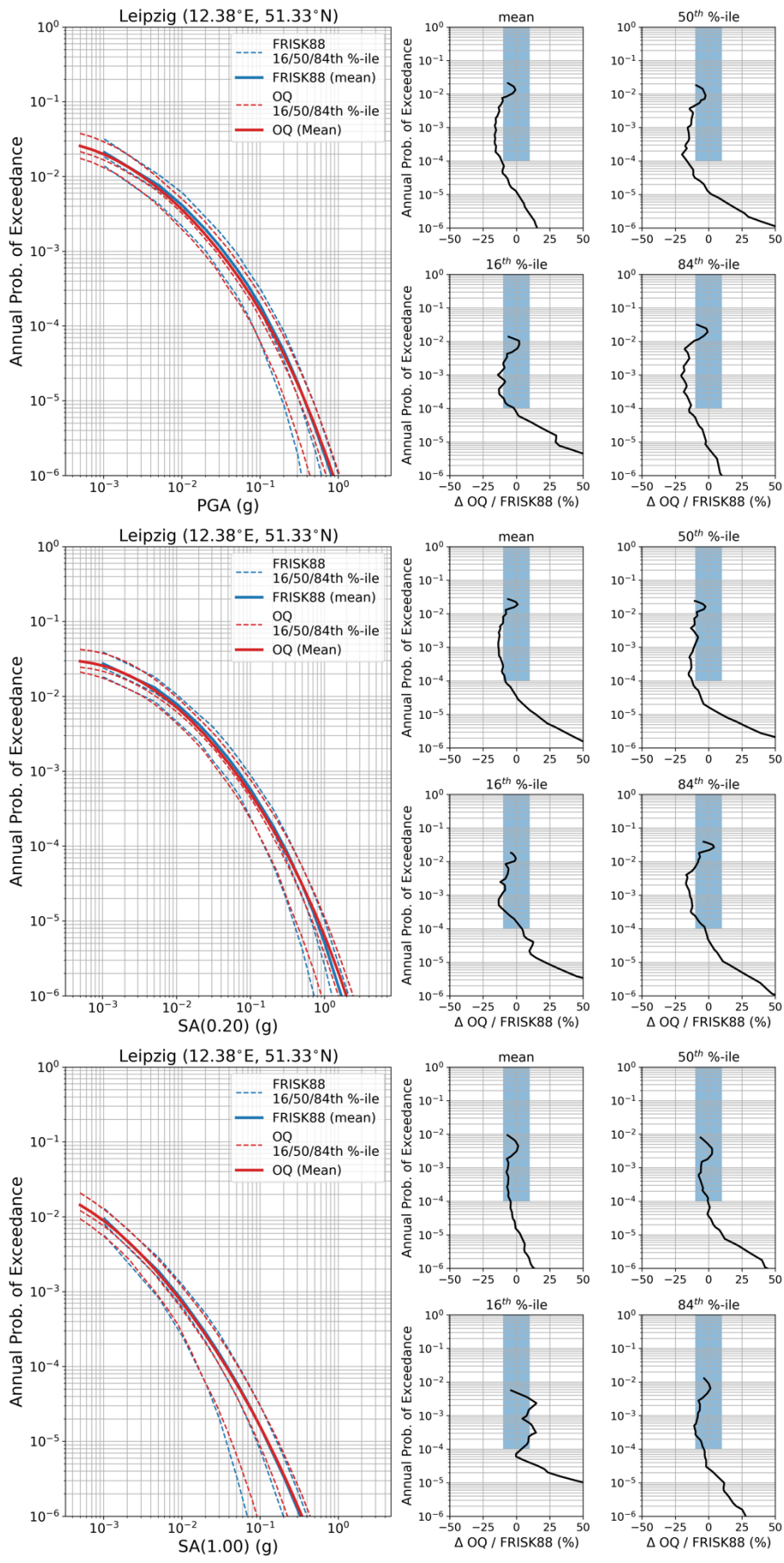
Figure S18. Leipzig (12.38°E, 51.33°N)
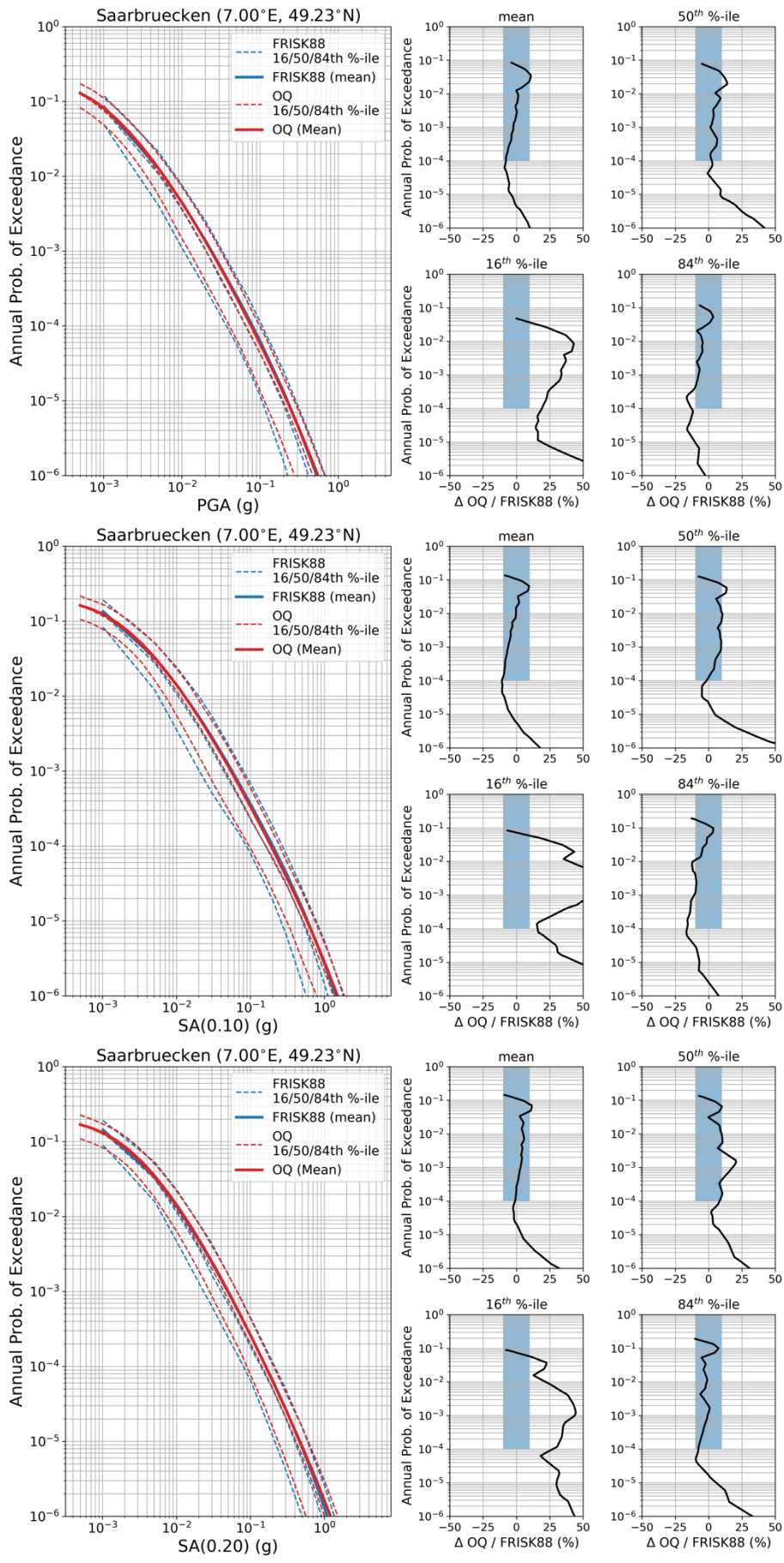
Figure S19. Saarbrücken (7.00˚E, 49.23˚N)